Short Communication

Visualization and characterization of gas–liquid mass transfer around a Taylor bubble right after the formation stage in microreactors

Lixia Yang [a,b,c,d,e,f], Nicolas Dietrich [a,b,c,f,*], Karine Loubière [d,e,f], Christophe Gourdon [d,e,f], Gilles Hébrard [a,b,c,f]

[a] Université de Toulouse, INSA, LISBP, 135 Av. de Rangueil, F-31077 Toulouse, France
[b] INRA UMR792, Ingénierie des Systèmes Biologiques et des Procédés, F-31400 Toulouse, France
[c] CNRS UMR 5504, Ingénierie des Systèmes Biologiques et des Procédés, F-31400 Toulouse, France
[d] Université de Toulouse, INPT, LGC, 4 Allée Emile Monso, F-BP 84234, 31432 Toulouse, France
[e] CNRS UMR 5503, Laboratoire de Génie Chimique, F-31432 Toulouse, France
[f] Fédération de Recherche FERMAT, CNRS, Toulouse, F-31400 Toulouse, France

HIGHLIGHTS

- Visualization of mass transfer around Taylor bubbles in microreactor.
- Contributions of the bubble formation stage to the overall gas–liquid mass transfer.
- The enhancement by the recirculation in the gas bubble at the formation stage was studied.
- New insight into bubble mass transfer right after the formation stage.
- Basis for elaborating a complete model, accounting for the bubble formation stage.

ABSTRACT

The gas–liquid mass transfer occurring in Taylor flows right after the bubble formation stage were investigated in a flow-focusing microreactor. The colorimetric technique proposed by Dietrich et al. (2013) was used for locally visualizing and characterizing the gas–liquid mass transfer. Thanks to this method, the liquid-side mass transfer coefficients k_L were measured at the moment right after the bubble is detaching from the gas film near the cross-junction of the microreactor. Experiments were carried out for several flow conditions ($95.7 < Re < 226.1, 0.0043 < Ca < 0.010, 0.4 < We < 2.3, Bo = 0.044$) and bubble size ($2.34 < L_b/l < 5.59$). The results have demonstrated that the contribution of mass transfer right after the bubble formation stage is reasonably larger to those obtained at the bubble flowing-stage.

Keywords:
Gas–liquid mass transfer
Taylor bubble
Formation stage
Microreactor
Colorimetric technique
Liquid-side mass transfer coefficient

1. Introduction

When compared with conventional reactors, microreactors present several advantages, such as high surface-to-volume ratio, excellent mass and heat transfer performances and narrow residence time distribution. Hence, they become an efficient technology for organic synthesis (Ehrfeld et al., 2000, Dietrich, 2011, Köhler and Cahill, 2014, Darvas et al., 2014). Gas–liquid reactions occupy a key place in scientific research and industrial application fields dealing with flow chemistry. In such systems, it is essential to perfectly characterize and control the mass transfer between both phases insofar as, depending on chemical kinetics, it can become the limiting step and thus induce a decrease of the chemical conversion or selectivity.

In recent years, gas–liquid flows in micro- and milli-channels have been the subject of an extensive literature (Garstecki et al., 2006; Dietrich et al., 2008; Pohorecki et al., 2008; Sobieszuk and Pohorecki, 2010; Zhao et al., 2010; Kashid et al., 2011; Roudet et al., 2011; Wang et al., 2013; Pan et al., 2014; Zhu et al., 2014; Kastens et al., 2015). Most of these works are devoted to the understanding and modeling of the hydrodynamics associated with the Taylor flows, as this kind of flow enables to achieve the best gas–liquid mass transfer rates required for implementing

* Corresponding author at: Université de Toulouse, 135 avenue de Rangueil, 31077 Toulouse, France. Tel.: +33 561559760; fax: +33 561559760.
E-mail address: Nicolas.Dietrich@insa-toulouse.fr (N. Dietrich).

http://dx.doi.org/10.1016/j.ces.2016.01.013

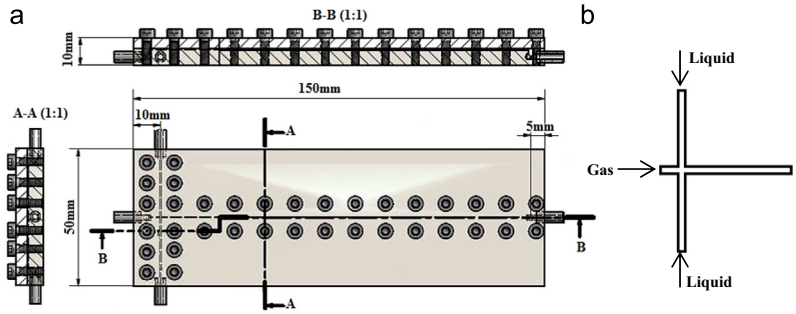

Fig. 1. (a) Geometry of the microchanel (Cross section: $A = l^2 = 500 \times 500\ \mu m^2$) and (b) schematic representation of the cross-junction.

gas–liquid reactions. When investigated, the gas–liquid mass transfer characteristics are globally measured, namely by analyzing the solute concentration of samples collected at the outlet of microreactors. Such a method might lead to an inaccurate characterization, the sample collection and phase separation times being not usually taken into account. Few studies have also studied the separate contribution to mass transfer of the three characteristic stages, which are the bubble-forming, the bubble-flowing and the phase separation ones. Herein, it is necessary to propose online direct and more local approach to overcome these limitations and to isolate the contribution of the different stages. In this perspective, Tan et al. (2012) and Yang et al. (2014) have recently developed in situ methods, based on the time-dependent variations of the bubble sizes, to investigate the mass transfer of bubbly flows in T-junction and/or co-flowing microchannels. These authors have demonstrated that the mass transfer during the formation stage contributes significantly to the overall transferred solute, in particular with respect to the associated short mass transfer times. At present, there exists no report dealing with the direct visualization of mass transfer at microscale and just after the bubble pinch-off. Dietrich et al. (2013) have proposed a colorimetric technique (based on an oxygen-sensitive dye and without any laser excitation) to study the gas–liquid mass transfer of bubbles flowing in a millimetric square channel. In keeping with this work, the present study aims at applying this method to visualize and quantify the gas–liquid mass transfer occurring right after the bubble formation stage in a flow-focusing microchannel.

2. Materials and methods

2.1. Principles of the colorimetric technique

The method used was the colorimetric technique proposed by Dietrich et al. (2013). Resazurin (CAS 62758-13-8, molecular mass: 229.19 g mol^{-1}) was chosen as the dye which reacts with oxygen in the presence of potassium hydroxide (KOH) and glucose solution. In the reduced form, named dihydroresorufin, the solution is colorless, while in presence of oxygen, the oxidized form, named resorufin, is characterized by an intense pink color. To make possible the visualization of the colored field, the kinetics for the oxidation reaction should be quasi-instantaneous and the kinetics of the back reaction slow (few minutes). For that, an optimal composition of the catalyzer was determined, taking into account the balance between the oxidation and reduction kinetics, and also the requirements in terms of adequate color intensity levels. This led to potassium hydroxide and glucose solutions both diluted at 30 g L^{-1} in deionized water (the conductivity of the deionized water is 51.2 µs m^{-1}), and to a concentration of resazurin fixed at 1 g L^{-1} ($\sigma_L = 55.6$ mN m^{-1}, $\mu_L = 1.12$ mPa s, $\rho_L = 1004.5$ kg m^{-3}). The latter concentration was 10 times larger than the one used by Dietrich et al. (2013) in order to conserve the same quality of images.

2.2. Description of the experimental set-up

The experimental set-up consisted of a straight horizontal channel of square cross section $A = l^2$ where $l = 500\ \mu m$ (4 times smaller than Dietrich et al. (2013)). The channel was curved in a polymethyl methacrylate (PMMA) plate (5 mm thick) and roofed over in a watertight manner by another plate (5 mm thick). The geometry of the channel is presented in Fig. 1.

Gas (air) and liquid phases (solution with dye, glucose and potassium hydroxide, flushed by nitrogen before the inlet of the channel) were both delivered from a 60 mL syringe in a syringe pump (Harvard Apparatus, PHD 22/2000, USA). Gas flow rates ranged from 0.6 to 1.2 mL min^{-1} and liquid flow rates from 2.4 to 4.0 mL min^{-1} in order to obtain a Taylor flow regime. The associated superficial gas j_G and liquid velocities j_L are: $0.040\ m\ s^{-1} \leq j_G = Q_G/l^2 \leq 0.080\ m\ s^{-1}$ and $0.160\ m\ s^{-1} \leq j_L = Q_L/l^2 \leq 0.267\ m\ s^{-1}$. All of the experiments were conducted at a room temperature of 293 K and atmospheric pressure.

2.3. Characterization of gas–liquid flow hydrodynamics and mass transfer

The shadowgraph method was applied to investigate the gas–liquid hydrodynamics and mass transfer inside the microchannel. The channel was lighted by a LitePad HO LED backlight (Rosco®) and the images were recorded by a monochromatic high-speed camera (Photron SA3) at 4000 frames per second. Image resolution was 10 µm per pixel and the region of interest $10 \times 1.5\ mm^2$. The software ImageJ (version 1.38e, National Institute of Health, USA) was used to analyze the recorded images. The following hydrodynamic characteristic parameters were measured: bubble length L_B, bubble velocity$U$, and the length of the unit cell L_{UC}.

The transfer of oxygen from air bubbles into resazurin solution was investigated over the range of gas and liquid flow rates defined in Section 2.2, which covered only the Taylor flow regime ($95.7 < Re < 226.1, 0.0043 < Ca < 0.010, 0.4 < We < 2.3, Bo = 0.044$). As the camera is monochromatic, the different levels of pink coloration taken by the dye solution, which depended only on the quantity of oxygen transferred, were represented by 255 gray levels on the acquired images.

The gas–liquid mass transfer characteristics were determined by an image post treatment algorithm implemented on the software Matlab (R2011b), as the one used by Dietrich et al. (2013). It consisted of two steps: (i) the determination of the calibration curve, and (ii) the image processing which enabled to transform the acquired gray-level images into the equivalent oxygen concentration fields. Note that the term “equivalent” is used as in reality the oxygen concentration is null as consumed by the instantaneous oxidation reaction. For the calibration process,

different concentrations of resazurin solution were prepared: 0, 0.35 g L^{-1}, 0.75 g L^{-1} and 1 g L^{-1}. The obtained calibration curve, depicted in Fig. 2a, shows that the linearity between the gray levels and the equivalent quantities of oxygen transferred per unit of liquid volume is conserved even if the employed concentration of resazurin is significantly increased.

In this study, a focus was made on the gas–liquid mass transfer occurring right after the bubble formation stage, namely at the moment right after the pinch-off stage (see Fig. 2b). In this case, by applying the method proposed by Dietrich et al. (2013), the liquid-side mass transfer coefficient right after the bubble formation stage k_L can be calculated by Eq. (1) (the oxygen concentration C is always equal to zero):

$$k_L = \frac{\overline{C_{mes}} \times j_L}{X \times a \times C^*} \quad (1)$$

where a is the interfacial area between gas and liquid phases, C^* the dissolved oxygen concentration at saturation (8.15 mg L^{-1}), X the axial location corresponding to the bubble pinch-off (see Fig. 2b) and $\overline{C_{mes}}$ the average equivalent oxygen concentration in the liquid slug of the unit cell at this location, deduced from image processing. It is important to notice that the equivalent oxygen concentration field obtained at a given location (x,y) is a mean value along the z-axis (Dietrich et al., 2013). This is a limitation of the present method: it does not enable to discriminate the equivalent oxygen concentration fields related to each xy-planes along the channel height. Meanwhile, as visualization of the bubble areas of the nose and rear due to the hemispheric shape is also not available, this liquid volume linked to these bubble areas cannot be taken into account for the calculation, this could lead to a maximum error of 18% on the volume estimation of liquid phase in a unit cell. An identical calculation was made for the complete unit cell flowing at a static axial location equal to 14 times the channel width from the junction corresponding to a bubble-flowing condition, by using $\overline{C_{mes}'}$ instead of $\overline{C_{mes}}$ (see Fig. 2c).

The interfacial area a was calculated by assuming a hemispherical shape for the bubble nose and rear, and a cylindrical shape for the bubble body. Typically, they were ranged from 3734 m^{-1} to 4884 m^{-1} in the operating domain investigated.

3. Results and discussion

The measured values of the length of the bubble L_B, the length of the liquid slug L_{slug}, the interfacial area a are listed in Table 1. As in Roudet et al., (2011), a correlation relating L_B/l to j_G/j_L has been found to be well adapted (mean relative deviation of 12.5%),

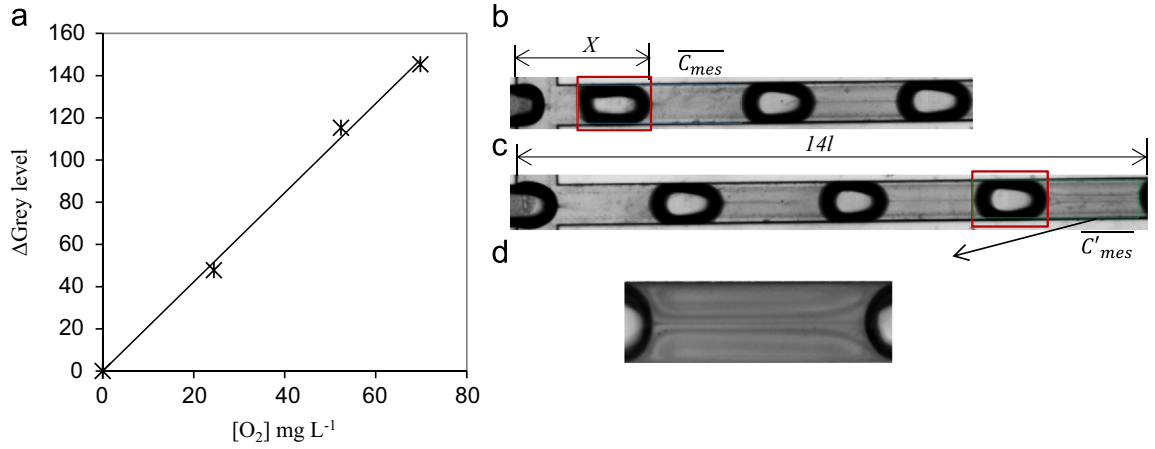

Fig. 2. (a) Calibration curve between gray levels and equivalent quantities of oxygen transferred per unit of liquid volume, (b) Illustration of the bubble right after pinch-off. $\overline{C_{mes}}$: average equivalent oxygen concentration in the liquied slug of the unit cell at this location (the blue rectangle); X: axial position of the bubble, $X=0$: the two phases enter in contact, (c) illustration of the comlete unit cell bubble flowing within distance equal to 14 times the channel width from the junction.$\overline{C'_{mes}}$: average equivalent oxygen concentration in the liquid slug of the unit cell at this location (the green rectangle). The bubbles in the red rectangle represetnt the bubble observed, (d) magnification obseravation of the mass transfer in the liquid slug.(For interpretation of the references to color in this figure legend, the reader is referred to the web version of this article.)

Table 1
Comparison of volumetric liquid-side mass transfer coefficient k_La and liquid-side mass transfer coefficient k_L at two positions, right after the pinch-off and for the complete unit cell flowing at a static location equal to 14 times the channel width from the junction. The superscript "' " notes the value for the latter situations.

Gas superficial velocity ($m\,s^{-1}$)	Liquid superficial velocity ($m\,s^{-1}$)	L_{slu} (mm)	L_B (mm)	a (m^{-1})	k_{La} (s^{-1})	k'_La (s^{-1})	$k \times 10^{-4}$ ($m\,s^{-1}$)	$k'_L \times 10^{-4}$ ($m\,s^{-1}$)
0.040	0.16	0.79	2.12	4577	6.27	4.11	13.70	8.98
	0.19	0.80	2.02	4501	6.62	4.27	14.70	9.49
	0.21	1.05	1.63	3822	6.08	3.58	15.90	9.37
	0.27	0.95	1.39	3740	6.47	3.90	17.30	10.40
0.067	0.16	0.77	2.37	4736	9.14	3.87	19.30	8.16
	0.19	0.67	2.34	4884	10.65	4.23	21.80	8.67
	0.27	1.06	1.17	3301	10.00	4.47	30.30	13.50
0.080	0.16	0.67	2.79	5073	11.67	6.51	23.00	12.80
	0.19	0.71	2.42	4864	13.23	7.02	27.20	14.40
	0.21	0.77	1.91	4480	15.28	8.27	34.10	18.50
	0.27	0.73	1.51	4233	17.10	8.87	40.40	20.90

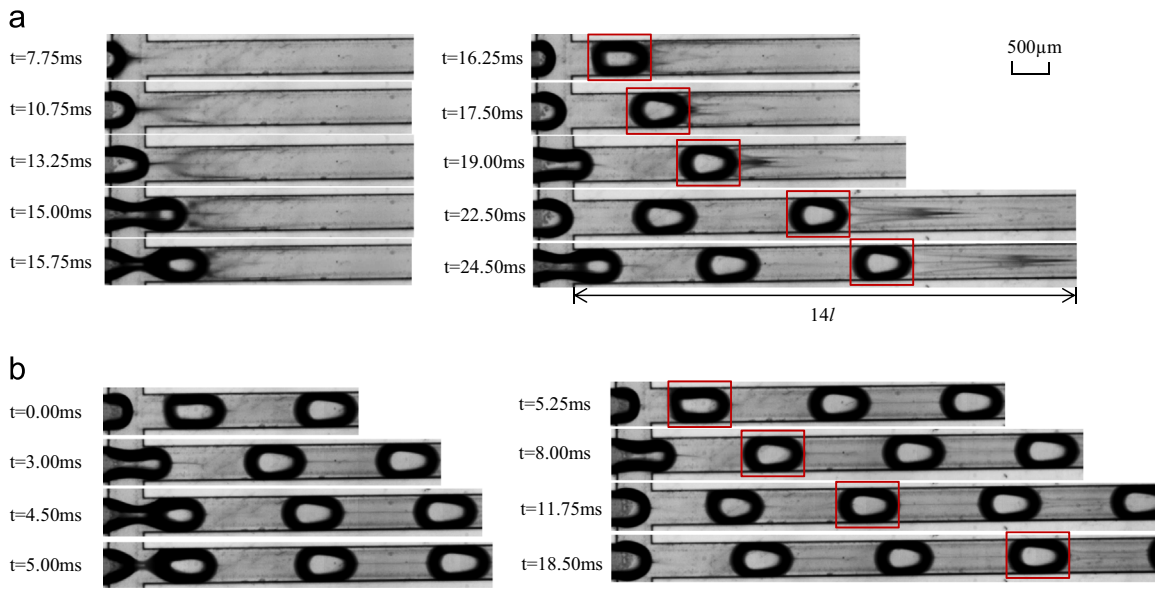

Fig. 3. Typical images of the mass transfer process (j_G=0.053 m s^{-1}, j_L=0.27 m s^{-1}). (a) Just after the moment where both gas and liquid phases are injected in the microchannel (transient period), and (b) when steady state is reached. The bubble in the red rectangle represents the bubble observed.(For interpretation of the references to color in this figure legend, the reader is referred to the web version of this article.)

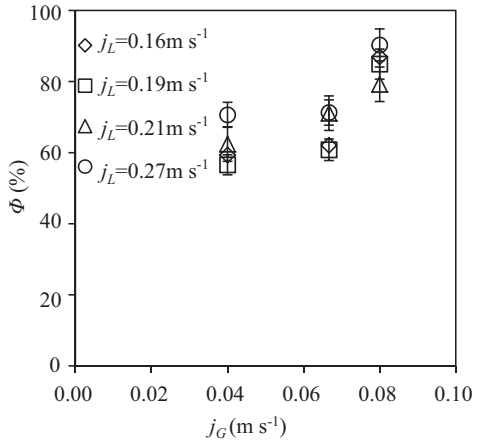

Fig. 4. Variation of the mass transfer amount fraction Φ as a function of the gas superficial velocity at different liquid superficial velocities.

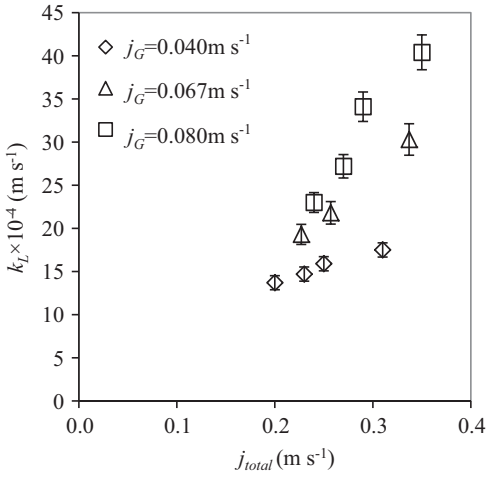

Fig. 5. Liquid side mass transfer coefficient kL versus the total superficial velocity (j_{total}=j_G+j_L) at different gas superficial velocities.

leading to:

$$\frac{L_B}{l} = 2.20 + 5.57\left(\frac{j_G}{j_L}\right) \quad (2)$$

Fig. 3a presents a typical image sequence obtained just after the moment where both gas and liquid phases are injected in the microchannel. It thus corresponds to the transient period during which the Taylor flow has not yet reached the steady-state regime. Fig. 3b reports, for the same superficial velocities, the image sequence obtained when the flow is steady. The comparison of both sequences reveals that for the first bubble entering in the microchannel, the equivalent oxygen concentration fields are clearer than when steady state is reached, and that oxygen almost accumulates in the front of the bubble. This can be explained by the fact that for the first bubble, no recirculation exists in the liquid phase, which slows down the mass transfer mechanism.

From image processing, the mass amount of oxygen in the liquid slug has been calculated right after the bubble pinch-off (m_{O_2}) and for the complete unit cell flowing at a static location equal to 14 times the channel width from the junction where the two phases began to contact (m'_{O_2}). From these two values, the mass transfer amount fraction, ϕ, defined by Tan et al. (2012) can be defined according to.

$$\varnothing = m_{O_2}/m'_{O_2} \quad (3)$$

Fig. 4 reports the variation of this fraction as a function of the gas superficial velocity j_G for different liquid superficial velocities. It can be seen that, at a given $_{jG}$, ϕ slightly increase when rising j_L, and for a given j_L, ϕ seems to globally increase as j_G increases. ϕ is in a range of 45–90% under the experimental conditions, which is larger than that (30–40%) in Tan et al. (2012). The explanation could be that both the gas–liquid flow rates are greater in this case, which can enhance the mass transfer during the formation stage, and thus the contribution of the formation stage to the total mass transfer.

The variation of liquid-side mass transfer coefficient k_L, obtained right after the bubble pinch-off (Eq. (1) with$\overline{C_{mes}}$) is plotted as a function of the total superficial velocity at different gas superficial velocities j_{total} in Fig. 5. It can be observed that: (1) j_{total}

has a positive effect on k_L, and at a fixed j_{total}, namely, k_L increases as j_L increases; (2) as the gas superficial increases, k_L increases. In addition, from Table 1, it demonstrates that for a fixed j_L, k_L increases as j_G increases. This phenomena is contrary to what observed by Dietrich et al. (2013), during the bubble flowing-stage, but agrees with the results of Tan et al. (2012) and Yang et al. (2014) obtained during the bubble formation stage. It could be explained by the fact that, due to the dynamic process of the bubble formation, the liquid films around the bubble is quickly renewed. In this case, the liquid-side mass transfer resistance becomes negligible when compared to the gas side resistance. Consequently, an increase of the gas flow rate improves the mixing (circulating flow) inside the forming bubble and thus the surface renewal in the bubble and the mass transfer.

In order to quantify the enhancement induced by the recirculation in the gas bubble, the enhancement factor E defined by Tan et al. (2012) was calculated according to

$$E = \frac{k_L}{k_{L,diff}} \tag{4}$$

$$k_{L,diff} = 2\sqrt{\frac{D_{O_2}}{\pi t}} \tag{5}$$

where $k_{L,diff}$ is the liquid-side mass transfer coefficient right after the bubble pinch-off defined considering the Higbie penetration model, D_{O_2} the oxygen diffusion coefficient (equal here to 1.75×10^{-9} m^2 s^{-1}), t the bubble formation time (ranged from 4.75 to 10.50 ms). The obtained E varies from 2 to 8 and is smaller than that the values of Tan et al. (2012) varying between 5 and 15. Such a difference is linked due to the fact that diffusion coefficient of CO_2 in NaOH solution in their case is greater than the one here involved, and also that the bubble formation times are larger (200–400 ms against 4.75–10.50 ms).

At last, Table 1 displays a comparison of volumetric mass transfer coefficients and liquid-side mass transfer coefficients at two locations, right after the pinch-off and for the complete unit cell flowing at a static location equals to 14 times the channel width from the junction. It illustrates that both the values of k_La and k_L are significantly larger right after the bubble formation (increase by 28–64% for k_La and by 28–65% for k_L). This confirms that the contribution of the mass transfer of the formation stage to the overall mass transfer is reasonably large when compared to the relatively short bubble formation times involved.

4. Conclusion

A colorimetric technique was applied to visualize and characterize the gas–liquid mass transfer in a square microchannel. Compared with the previous work (Dietrich et al., 2013), this study demonstrated that this technique can also be feasible at micron scale. A focus was made on the local characterization of gas–liquid mass transfer at the bubble formation stage. The results obtained showed that the bubble formation stage made a reasonably large contribution (45–90% for the complete unit cell flowing at a static location equals to 14 times the channel width from the junction) to the mass transfer of overall flowing-stage when compared to the relatively short bubble formation times (4.75–10.50 ms). The liquid-side mass transfer coefficient during the formation stage was intensified by 2–8 times due to the enhancement of the mixing inside the forming bubble. All these findings give important information to understand the contributions of the bubble formation stage to the overall gas–liquid mass transfer occurring in a microchannel. In the future, they will serve as basis for elaborating a complete model, accounting for the bubble formation stage.

Nomenclature

Greek letters

μ_L	dynamic viscosity (Pa s)
ρ_L	density (kg/m^3)
σ_L	surface tension (N/m)

Dimensionless numbers

Re	Reynolds number ($Re = \frac{\rho_L \times U \times l}{\mu_L}$)
Ca	Capillary number ($Ca = \frac{\mu_L \times U}{\sigma_L}$)
We	Weber number ($We = \frac{\rho_L \times U^2 \times l}{\sigma_L}$)
Bo	Bond number ($Bo = \frac{\rho_L \times l^2 \times g}{\sigma_L}$)

References

Darvas, F., Dorman, G., Hessel, V., 2014. Flow chemistry. Boston : De Gruyter Textbook, Berlin.

Dietrich, N., Loubière, K., Jimenez, M., Hébrard, G., Gourdon, C., 2013. A new direct technique for visualizing and measuring gas–liquid mass transfer around bubbles moving in a straight millimetric square channel. Chem. Eng. Sci. 100, 172–182. http://dx.doi.org/10.1016/j.ces.2013.03.041.

Dietrich, N., Poncin, S., Midoux, N., Li, H.Z., 2008. Bubble formation dynamics in various flow-focusing microdevices. Langmuir 24, 13904–13911. http://dx.doi.org/10.1021/la802008k.

Dietrich, T., 2011. Microchemical Engineering in Practice. Wiley-VCH, Weinheim.

Ehrfeld, W., Hessel, V., Lowe, H., 2000. Microreactors: New Technology for Modern Chemistry. Wiley-VCH, Weinheim.

Garstecki, P., Fuerstman, M.J., Stone, H. a, Whitesides, G.M., 2006. Formation of droplets and bubbles in a microfluidic T-junction-scaling and mechanism of break-up. Lab. Chip 6, 437–446. http://dx.doi.org/10.1039/b510841a.

Kashid, M.N., Renken, A., Kiwi-Minsker, L., 2011. Gas–liquid and liquid–liquid mass transfer in microstructured reactors. Chem. Eng. Sci. . http://dx.doi.org/10.1016/j.ces.2011.05.015

Kastens, S., Hosoda, S., Schlüter, M., Tomiyama, A., 2015. Mass transfer from single taylor bubbles in minichannels. Chem. Eng. Technol. 38, 1925–1932. http://dx.doi.org/10.1002/ceat.201500065.

Micro-Segmented Flow, Biological and Medical Physics. In: Köhler, J.M., Cahill, B.P. (Eds.), Biomedical Engineering. Springer Berlin Heidelberg, Berlin, Heidelberg http://dx.doi.org/10.1007/978-3-642-38780-7.

Pan, Z., Zhang, X., Xie, Y., Cai, W., 2014. Instantaneous mass transfer under gas–liquid taylor flow in circular capillaries. Chem. Eng. Technol. 37, 495–504. http://dx.doi.org/10.1002/ceat.201300354.

Pohorecki, R., Sobieszuk, P., Kula, K., Moniuk, W., Zielinski, M., Cyganski, P., Gawinski, P., 2008. Hydrodynamic regimes of gas–liquid flow in a microreactor channel. Chem. Eng. J. 135, S185–S190. http://dx.doi.org/10.1016/j.cej.2007.07.039.

Roudet, M., Loubiere, K., Gourdon, C., Cabassud, M., 2011. Hydrodynamic and mass transfer in inertial gas–liquid flow regimes through straight and meandering millimetric square channels. Chem. Eng. Sci. 66, 2974–2990. http://dx.doi.org/10.1016/j.ces.2011.03.045.

Sobieszuk, P., Pohorecki, R., 2010. Gas-side mass transfer coefficients in a falling film microreactor. Chem. Eng. Process. Process. Intensif. 49, 820–824. http://dx.doi.org/10.1016/j.cep.2010.06.010.

Tan, J., Lu, Y.C., Xu, J.H., Luo, G.S., 2012. Mass transfer characteristic in the formation stage of gas–liquid segmented flow in microchannel. Chem. Eng. J. 185, 314–320. http://dx.doi.org/10.1016/j.cej.2012.01.054.

Wang, X., Yong, Y., Yang, C., Mao, Z.-S., Li, D., 2013. Investigation on pressure drop characteristic and mass transfer performance of gas–liquid flow in microchannels. Microfluid. Nanofluidics 16, 413–423. http://dx.doi.org/10.1007/s10404-013-1226-5.

Yang, L., Tan, J., Wang, K., Luo, G., 2014. Mass transfer characteristics of bubbly flow in microchannels. Chem. Eng. Sci. 109, 306–314. http://dx.doi.org/10.1016/j.ces.2014.02.004.

Zhao, Y., Su, Y., Chen, G., Yuan, Q., 2010. Effect of surface properties on the flow characteristics and mass transfer performance in microchannels. Chem. Eng. Sci. 65, 1563–1570. http://dx.doi.org/10.1016/j.ces.2009.10.027.

Zhu, C., Li, C., Gao, X., Ma, Y., Liu, D., 2014. Taylor flow and mass transfer of CO_2 chemical absorption into MEA aqueous solutions in a T-junction microchannel. Int. J. Heat. Mass. Transf. 73, 492–499. http://dx.doi.org/10.1016/j.ijheatmasstransfer.2014.02.040.